Title:

CRIPTO promotes extracellular vesicle uptake and activation of fibroblasts exposed to triple negative breast cancer cells

Authors:

David W. Freeman[1,2], Brooke L. Gates[1,2], Mauri D. Spendlove[1], H. Evin Gulbahce[3], Benjamin T. Spike[1,2]

1. Huntsman Cancer Institute, University of Utah, Salt Lake City, UT 84112, USA
2. Department of Oncological Sciences, University of Utah, Salt Lake City, UT 84112, USA
3. Department of Pathology and Laboratory Medicine, Huntsman Cancer Institute, University of Utah Health, Salt Lake City, UT 84112, USA

*Correspondence: Benjamin.spike@hci.utah.edu

Keywords: Breast Cancer, Cancer Associated Fibroblasts, Extracellular Vesicles, CRIPTO, Tumor Microenvironment

ABSTRACT

Expression of CRIPTO, a factor involved in embryonic stem cells, fetal development, and wound healing, is tied to poor prognosis in multiple cancers. In previous models of triple negative breast cancer (TNBC), CRIPTO blockade inhibits tumor growth and dissemination. Here, we describe a novel mechanism by which CRIPTO-laden tumor extracellular vesicles (TEVs) facilitate reciprocal crosstalk between tumor cells and fibroblasts that drives aggressive TNBC phenotypes. CRIPTO expression in TNBC cells was required to program fibroblasts towards a cancer associated fibroblasts cell-state that promoted tumor cell invasion. TEVs bearing CRIPTO increased SMAD2/3 activation and TEV uptake in target fibroblasts through NODAL-dependent and -independent mechanisms, respectively. *In vivo*, CRIPTO levels dictated TEV uptake in the mouse lung, a site of EV-regulated premetastatic niches important for breast cancer dissemination. These discoveries highlight CRIPTO's potential to coordinate heterotypic cellular crosstalk through a previously unrecognized mechanism with implications for development, metastasis, and drug delivery.

INTRODUCTION

Tumors are comprised of an intricate network of parenchymal and stromal cells, whose intercellular signaling dictates cell state change, resistance to therapy, and tumor growth at both primary and distant sites[1]. Deciphering the molecular underpinnings of coordinate heterotypic signaling in these multi-cellular tumor microenvironments (TME) is crucial for understanding tumor progression and could uncover effective therapeutic strategies aimed at non-autonomous drivers of cancer progression and metastasis.

CRIPTO is a small GPI-anchored signaling protein encoded by the *TDGF1* gene that is prominently expressed in stem cells and early development, largely undetectable in adult homeostatic tissue, but reexpressed in the context of oncogenesis and wound healing[2]. In mammary developmental studies, inhibition of CRIPTO with a soluble CRIPTO ligand trap, Alk4^{L75A}-Fc (A4Fc), significantly impaired the multipotency of murine mammary stem cells and their proliferative renewal capacity[3]. Elevated CRIPTO is detectable in nearly 80% of breast cancers and its overexpression in upwards of 50% of invasive breast tumors is associated with poor prognosis and advanced disease states[4,5]. Knocking down CRIPTO, blocking its signaling with A4Fc, or delivering toxic payloads to CRIPTO expressing cells with an antibody-drug conjugate reduces primary tumor growth and distant metastasis in triple negative breast cancer (TNBC) xenograft models[6,7].

CRIPTO signaling is multifaceted[2,8]. It acts as a pivotal intermediary in cellular signaling by modulating the TGF-β pathway and independent pathways that activate c-Src/MEK/AKT[9]. In TGF-β signaling, it acts as an obligate co-receptor for the TGF-β family ligand NODAL while attenuating ACTIVIN and TGF-β activity[10-12]. Mechanisms of CRIPTO's growth factor-like signaling remain to be clarified. CRIPTO signaling is potentiated by direct interaction with cell-surface GRP78[13].

During periods of cellular stress, a fraction of GRP78 relocalizes from the endoplasmic reticulum – where it functions as a key regulator of the unfolded protein response – to the cell surface. This relocalization positions CRIPTO signaling as part of a microenvironment-responsive signaling axis. Within breast cancer xenograft models, we have shown CRIPTO and GRP78 co-localize along stressed hypoxic tumor margins, where A4Fc inhibits cell proliferation[7].

Though CRIPTO is known to act both autonomously *and* as a soluble secreted factor, it has been studied in cancer primarily as an autonomous factor within the epithelial tumor parenchyma. However, there is good reason to suspect CRIPTO may coordinate the activity of multiple cooperating cell types. Patients with cirrhotic livers have elevated levels of CRIPTO and alpha-smooth muscle actin (αSMA) expression, and similar patterns are seen in fibrotic remodeling after myocardial infarction[14]. We previously showed CRIPTO is distributed throughout the stromal environment in developing mammary rudiments, and is a crucial mediator of augmented proliferative potential of mammary stem cells when co-cultured with fibroblasts, suggesting a broader regulatory role in multicellular cooperation during tissue morphogenesis[3].

The interaction of heterotypic cells is critical in cancer. For instance, breast cancer associated fibroblasts (CAFs) facilitate treatment resistance, tumor proliferation, and enable metastatic outgrowth, partly through mechanical alterations of the ECM and cytokine secretion. They are one of the most abundant cell types in the tumor microenvironment (TME) and are thought to originate primarily from resident mammary fibroblasts, with potential contributions from mesenchymal stem cells[1]. The diversity of CAFs is influenced by molecular and pathological subtypes, intratumor spatial patterning, and microenvironmental cues like hypoxia. Though critical aspects of their interactions with parenchymal tumor cells hold high potential for therapeutic manipulation, the interactions are complex, and key targetable regulators remain to be identified[15-17].

91 Here, we demonstrate that CRIPTO governs a novel communication axis between tumor cells
92 and fibroblasts involving extracellular vesicles (EVs). This discovery emerged from our analysis
93 of single cell profiles of the TNBC cell line, MDA-MB-468. Specific subpopulations of MDA-MB-
94 468 cells were found to be CRIPTO dependent and correlate with CAF levels in patients, though
95 the signatures are distinct from classic EMT or CAF signatures. Enriched gene categories
96 included vesicular trafficking and extracellular vesicle programs. Together, these observations
97 prompted us to evaluate CRIPTO-mediated tumor cell-fibroblast crosstalk and the potential role
98 of EVs.
99
100 EVs are secreted mediators of intercellular crosstalk capable of shuttling proteins, DNA/RNA,
101 lipids, and various metabolites. Classically, EVs have been divided into three classes: (1)
102 Exosomes formed through endocytic intermediates, (2) Microvesicles produced through outward
103 membrane blebbing, and (3) Apoptotic bodies generated from dying cells[18]. Roles for EVs in tumor
104 initiation and progression have been described, including their capacity to prime pre-metastatic
105 niches in distant organs for tumor cell colonization[19]. We demonstrate that tumor cell derived
106 CRIPTO can foster fibroblast programming through paracrine signaling via extracellular vesicles
107 (EVs).
108
109 Mechanistically, CRIPTO-laden EVs can activate NODAL signaling in target fibroblasts while
110 exhibiting elevated NODAL-independent EV uptake *in vitro,* as well as elevated uptake in lungs
111 of mice where EVs have been implicated in the formation of pre-metastatic niches through
112 fibroblast modification. This discovery represents a key milestone in understanding CRIPTO
113 activity in multicellular contexts, including tumor microenvironments where CRIPTO-dependent
114 EV signaling could represent a novel therapeutic target for breast cancer and beyond.
115
116 **RESULTS**

117 **Tumor cell derived CRIPTO activity correlates with cancer associated fibroblast (CAF)**
118 **levels and patient outcomes**
119 We previously showed that CR1 antagonism by A4Fc limits various phenotypes in TNBC cells
120 associated with stemness and tumor progression, including the capacity of TNBC (MDA-MB-468)
121 organoids to undergo serial passaging without overt pre-passage organoid phenotypes[7]. This
122 suggested CRIPTO may regulate the maintenance of a stem-like cell population required for
123 secondary organoid outgrowth[7]. To test this, we performed single cell RNA-sequencing (scRNA-
124 seq) of MDA-MB-468 organoids transduced with an empty tet-inducible lentiviral expression
125 cassette ($s14^{Con}$) or a construct with inducible expression of secreted A4Fc ($s14^{A4Fc}$). Inhibition of
126 CRIPTO with A4Fc induced a marked skewing in two specific cell subpopulations (denoted cluster
127 5 and 8) (**Fig 1A)**. $s14^{A4Fc}$ cultures showed a marked loss of cluster 8 cells and an increase in
128 cluster 5 cells relative to $s14^{Con}$ cultures. We identified differentially expressed genes (DEGs)
129 representing these populations and confirmed CRIPTO dependency of select targets using
130 *TDGF1* knockdown (shCr) (**Fig 1B,C)**.
131
132 To help identify underlying biology regulated by CRIPTO in this setting, we examined the
133 enrichment of DEGs associated with these subpopulations in curated biological processes and
134 cellular compartment gene sets. Genes characteristic of cluster 8 showed enrichment in factors
135 predicted to localize to extracellular vesicles (EV) and exosomes **(Fig 1D, Fig S1A,B)**. Though
136 somewhat unexpected based on CRIPTO's role as a cell surface co-receptor, this link between
137 CRIPTO and EV biology was consistent with punctate staining we previously observed for
138 CRIPTO in tumor and developmental settings[3], unpublished proteomics work from our group
139 analyzing A4Fc pulldowns from xenografts indicating associated EV-markers, and recent reports
140 of CRIPTO expression in EVs from cholangiocarcinoma patients[7,20].
141

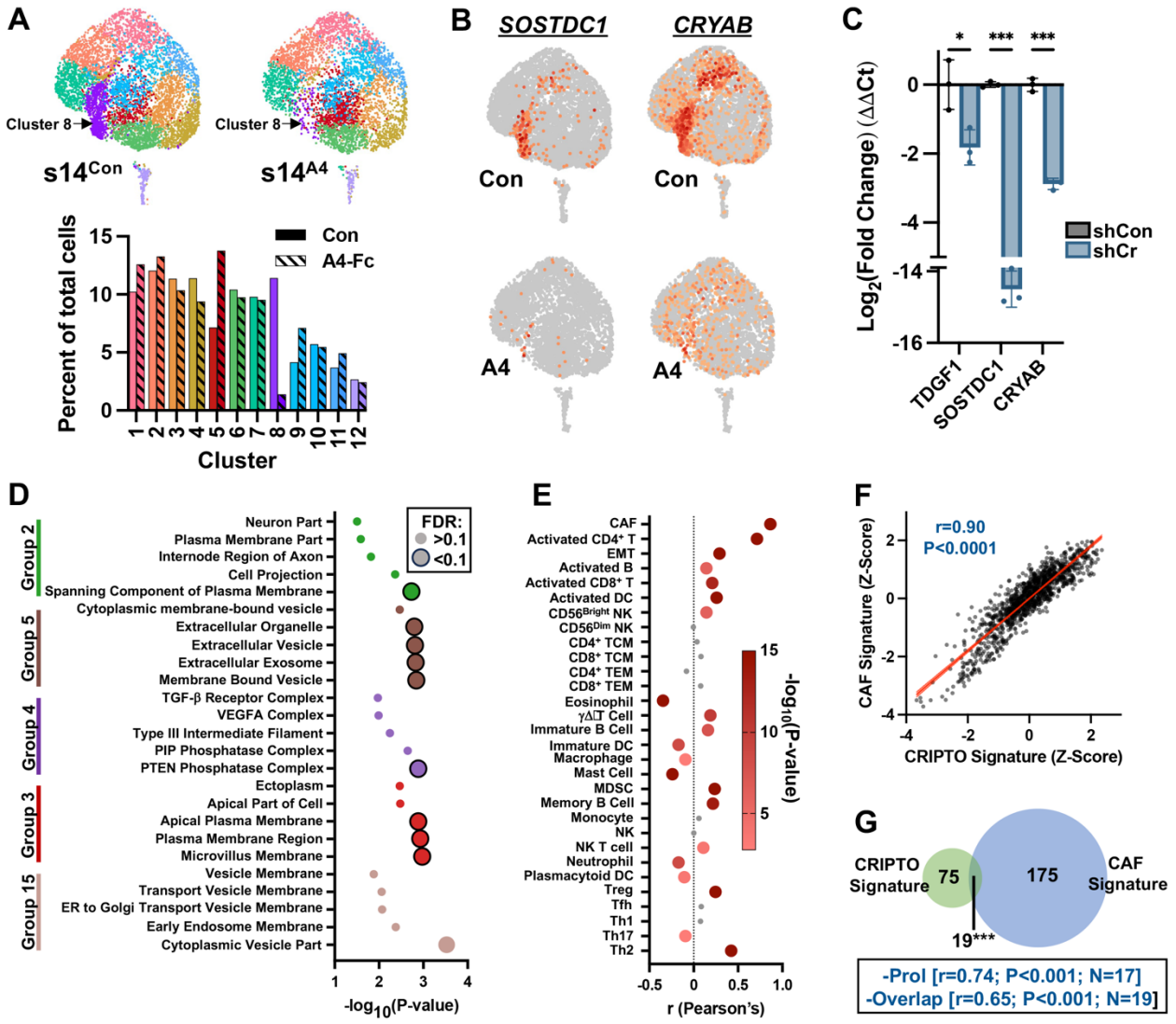

Figure 1. CRIPTO regulates TNBC tumor cell populations associated with extracellular vesicles and CAFs (A) UMAPS and relative cluster proportions of scRNA-seq of MDA-MB-468 s14^{Con} and s14^{A4Fc} organoids. (B) Representative genes enriched in cluster 8 and (C) validated by RT-qPCR in MDA-MB-468 shCon and shCr 2D cultures; Holm-Šidák Multiple T-tests. (B) Jensen cell compartment analysis of cluster 8 DEGs. Common compartments are clustered together, top 5 compartments for each enriched cluster are shown. Larger bubbles represent significantly enriched compartments (q<0.1; Benjamini-Hochberg). (E) Pearson's correlation of CRIPTO signature with stromal cell type gene signatues, larger bubbles represent significant correlations (Bonferonni adjusted P<0.0017) (H) Pearson's correlation between TDGF1 signature and CAF signature (TCGA). (I) Overlap of genes between CAF and gene signature (Hypergeometric distribution). Resulting Pearson correlations and P-values when genes in common or gene annotated as 'proliferation' by GO analysis were removed from the TCGA and CAF signatures. *P<0.05, ***P<0.00

142

143 Given the role of EVs as critical signaling mediators between tumor cells and tumor-supportive

144 stroma, we investigated whether EVs drive 'call and response' programs between CRIPTO-

145 regulated tumor cell populations and TME cell types[19,21]. First, we generated a composite gene

146 signature (CRIPTO Signature) for cluster 8 and cluster 5 reflecting tumor cell states under
147 CRIPTO's influence and assessed its correlation with TME cell populations using TCGA data (**Fig**
148 **1E, Table S1**)[22,23]. The CRIPTO signature was overexpressed in TNBC relative to other subtypes
149 and among stromal signatures in the TCGA database, was most strongly correlated with a CAF
150 gene signature, an association that persisted even after adjusting for the modest number of
151 shared genes between the signatures and proliferation-related genes (**Fig 1E-G; Fig S1C-E)**.
152 These findings are consistent with a CRIPTO-regulated tumor subpopulation influencing stromal
153 fibroblast programs within the TME.
154
155 **CRIPTO drives EV uptake by recipient fibroblasts**
156 Recent studies have identified CRIPTO in tumor-derived EVs (TEVs) in several cancer types[20,24].
157 To determine whether CRIPTO was likely to be present in EVs within the TME of breast cancers
158 in our system, we reanalyzed MDA-MB-468 xenograft tumors for expression and localization of
159 CRIPTO and the canonical EV marker CD81[25]. CRIPTO colocalized with CD81 in discrete
160 punctate structures along hypoxic tumor borders of MDA-MB-468 xenografts, where we
161 previously observed CRIPTO-dependent tumor cell phenotypes (**Fig 2A**)[7].
162
163 Indeed, isolated EVs from conditioned media of shCon MDA-MB-468 *in vitro* cultures exhibited
164 no obvious difference in canonical EV markers, size distribution, production quantity, or
165 morphology from EVs isolated from shCr cultures (**Fig 2B-D**). Nevertheless, timelapse
166 microscopy of $s14^{Con}$- and $s14^{A4Fc}$-expressing fibroblasts treated with fluorescently labeled TEVs
167 produced from shCon or shCr MDA-MB-468 cells demonstrated marked differences in EV uptake.

168 shCr EVs were internalized at lower rate compared to shCon in s14^{Con} cells and expression of

169 A4Fc in recipient fibroblasts reduced the uptake of shCon EVs (**Fig 2E**).

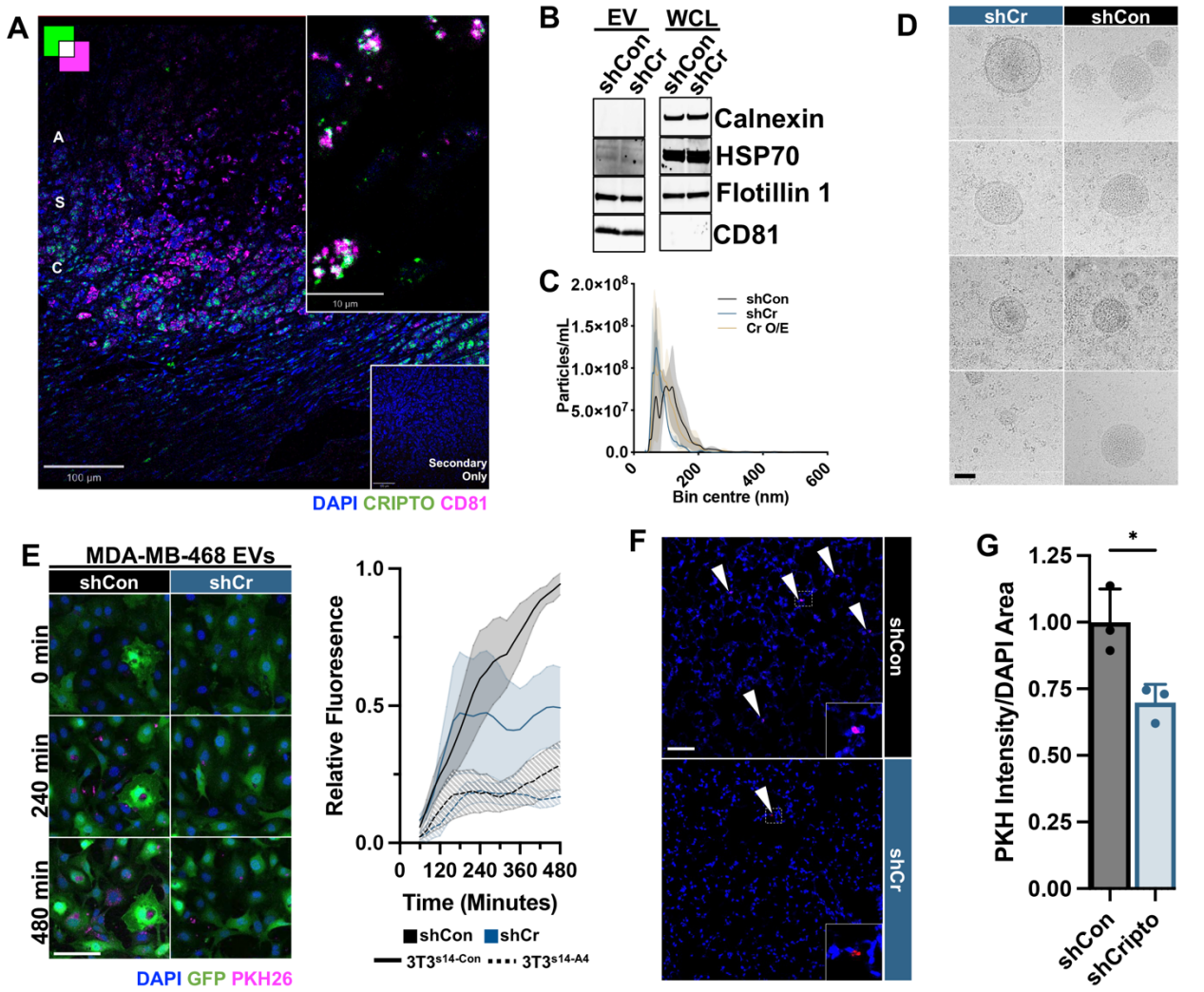

Figure 2. CRIPTO promotes EV uptake *in vitro* and *in vivo*
(A) Immunofluorescence of CD81 and CRIPTO in MDA-MB-468 xenograft tumor; A= acellular, S= stressed and C= cellular. Purity of TEVs isolated from MDA-MB-468 shCon and shCr by (B) Western blot, (C) Nanoparticle tracking analysis and (D) Cryo-electron microscopy, scale bar = 50nm. (E) Representative images and moving average intensity of 3T3$^{s14\text{-}Con}$ or 3T3$^{s14\text{-}A4}$ cells treated with TEVs from MDA-MB-468 shCon or shCr cells Scale Bar=100□m. (F) Representative images and (G) Quantification of PKH intensity/cell of lungs from mice treated with either PKH26 labeled EVs isolated from shCon, or shCr cells (N=3 animals/group; 5 field of views/animal). Two-tailed student's T-test, *P<0.05.

170

171 We next asked whether CRIPTO regulates EV uptake *in vivo* in mouse lungs where premetastatic

172 niches governed by EVs have been described and where we previously saw a drastic reduction

173 in metastasis of the TNBC cell line MDA-MB-231 when CRIPTO was blocked by A4Fc[7,19]. Thus,

174 we performed retroorbital injections of PKH26-labeled EVs isolated from shCon and shCr MDA-
175 MB-231 cells and analyzed lung tissue 24 hours later. We observed EV uptake by rare cells
176 throughout the lung in each case but noted that EVs from shCr cells exhibited significantly lower
177 levels of uptake in the lungs than EVs from shCon cells (**Fig 2F,G**). Collectively, these data point
178 towards a previously unidentified role for CRIPTO in enhancing EV uptake.
179
180 **Paracrine CRIPTO signaling promotes reciprocal tumor:fibroblast crosstalk**
181 To understand the effects of paracrine CRIPTO signaling via EVs on fibroblast activity, we first
182 reexamined TNBC xenograft tumors expressing $s14^{Con}$ of $s14^{A4Fc}$ in which we had originally
183 reported effects of A4Fc on tumor cell aggressiveness and disease progression, focusing now on
184 the TME rather than the tumor parenchyma[7]. Consistent with a role for CRIPTO in regulating CAF
185 activity, we noted alterations in collagen deposition under CRIPTO inhibition by A4Fc and
186 qualitative changes in stromal cell morphology and expression of αSMA (**Fig. S2A-B**). Similarly,
187 PDX models showing greater enrichment for the CRIPTO signature also scored higher for overall
188 fibrosis (**Fig 3A,B**), collectively suggesting a functional relationship between CRIPTO signaling
189 and CAF activity.
190
191 To functionally interrogate CRIPTO-dependent coordination of tumor cell and fibroblast interaction
192 in a controlled setting, we generated heterotypic organoid co-cultures of MDA-MB-468 cells and
193 growth-arrested 3T3 fibroblasts expressing $s14^{Con}$ or $s14^{A4Fc}$ In microwell cultures, incorporation
194 of $s14^{Con}$-fibroblasts stimulated tumor cell and fibroblast co-migration out of the well nadir,
195 whereas A4Fc expression reduced tumor cell migration despite no appreciable difference on
196 fibroblast movement (**Fig 3C**). Related experiments using transwell invasion assays confirmed
197 that the migratory phenotype in tumor cells was at least partly driven by soluble paracrine
198 signaling and involved tumor cell-dependent reprogramming of fibroblast cell state for reciprocal
199 promotion of tumor cell migration. That is, when naïve tumor cells were cultured above either

naïve s14^{Con} or s14^{A4Fc} fibroblasts over 48hrs, they migrated through Matrigel and the boundary membrane at low and comparable rates. However, primed fibroblasts (i.e. those previously exposed to tumor cells for a period of 3 days) dramatically enhanced the invasion of naïve tumor cells over 48 hours, and this was significantly reduced by A4Fc (**Fig 3D**). This migratory effect extended to organoid cultures of Patient Derived Xenografts (PdxOs) that endogenously expressed CRIPTO at different levels (**Fig 3D-E, Fig S2C**).

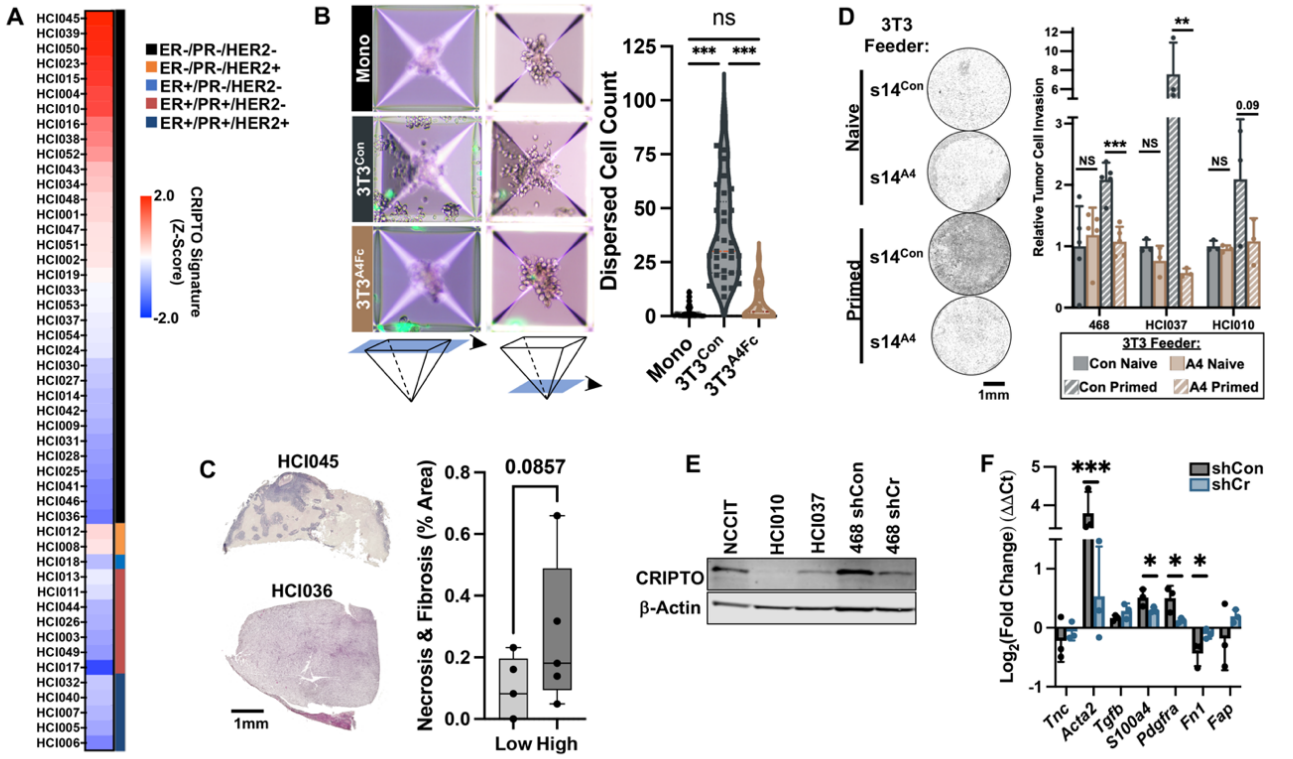

Figure 3. CRIPTO programs fibroblast differentiation through heterotypic paracrine signaling
(A) Relative CRIPTO signature across PDXs (B) Representative CRIPTO signature-high and –low PDX sections, quantification of necrotic and fibrotic area; N=5, Student's T-Test. (C) Representative photos and quantification of MDA-MB-468 spheroids grown with or without 3T3$^{s14\text{-}Con}$ or 3T3$^{s14\text{-}A4}$ fibroblasts in low adhesion microwells. One well=400□m. N=3 (10 microwells/biological replicate); One-way ANOVA with Tukey's multiple comparisons. (D) Transwell invasion assay of MDA-MB-468, HCI010, and HCI037 TNBC cells grown above 3T3$^{s14\text{-}Con}$ or 3T3$^{s14\text{-}A4}$ fibroblasts; two-way ANOVA Šidák Multiple Comparison. (E) Western blot of CRIPTO expression across cell models. (F)) RT-qPCR of CAF marker genes in 3T3 fibroblasts treated with conditioned media from shCon or shCr MDA-MB-468 cells. Fold change relative to 3T3 cells treated with autologous conditioned media; Student T-test. *P<0.05 , **P<0.01, ***P<0.001

We also examined canonical CAF markers by RT-qPCR following treatment of 3T3 fibroblasts with tumor cell conditioned media (CM). Repeated treatment with CM for 3 days from shCon cells altered the expression of CAF markers relative to fibroblasts treated with autologous conditioned

210 media, whereas these changes were attenuated when treating with CRIPTO knockdown CM (**Fig**
211 **3F**). Together, these data indicate tumor cell CRIPTO is indispensable in directing fibroblast
212 reprogramming through soluble paracrine signaling.
213
214 **EVs facilitate fibroblast activation through intercellular CRIPTO:NODAL signaling**
215 We next examined TEVs as possible mediators of paracrine CRIPTO signaling and fibroblast
216 programming. SMADs play a key role in CAF activation and are regulated by various TGF-β family
217 ligands and CRIPTO[12,26]. We, therefore, investigated SMAD2/3 activation in fibroblasts as a
218 function of paracrine signaling by CRIPTO-bearing TEVs. Conditioned media from control MDA-
219 MB-468 cells potently induced SMAD2/3 phosphorylation in fibroblasts, and the activity was
220 specifically associated with the isolated EV fraction of the control cell CM, while it was absent
221 from EV depleted fractions and from both fractions of EVs isolated from shCRIPTO cells (**Fig 4A**).
222 This implicates TEVs as the predominant signaling mechanism mediating non-autonomous
223 CRIPTO signaling between tumor cells and fibroblasts.
224
225 CRIPTO acts through ALK4 in conjunction with various TGF-β family ligands to modulate
226 SMAD2/3 activation[11]. We confirmed the invovment of ALK4,5,7 receptor complexes in CRIPTO
227 mediated SMAD2/3 activation in fibroblasts using pharmacological inhibition (SB431542).
228 ALK4,5,7 inhibition in fibroblasts blocked pSMAD2/3 increases following treatment with shCon
229 TEVs (**Fig 4B**).
230

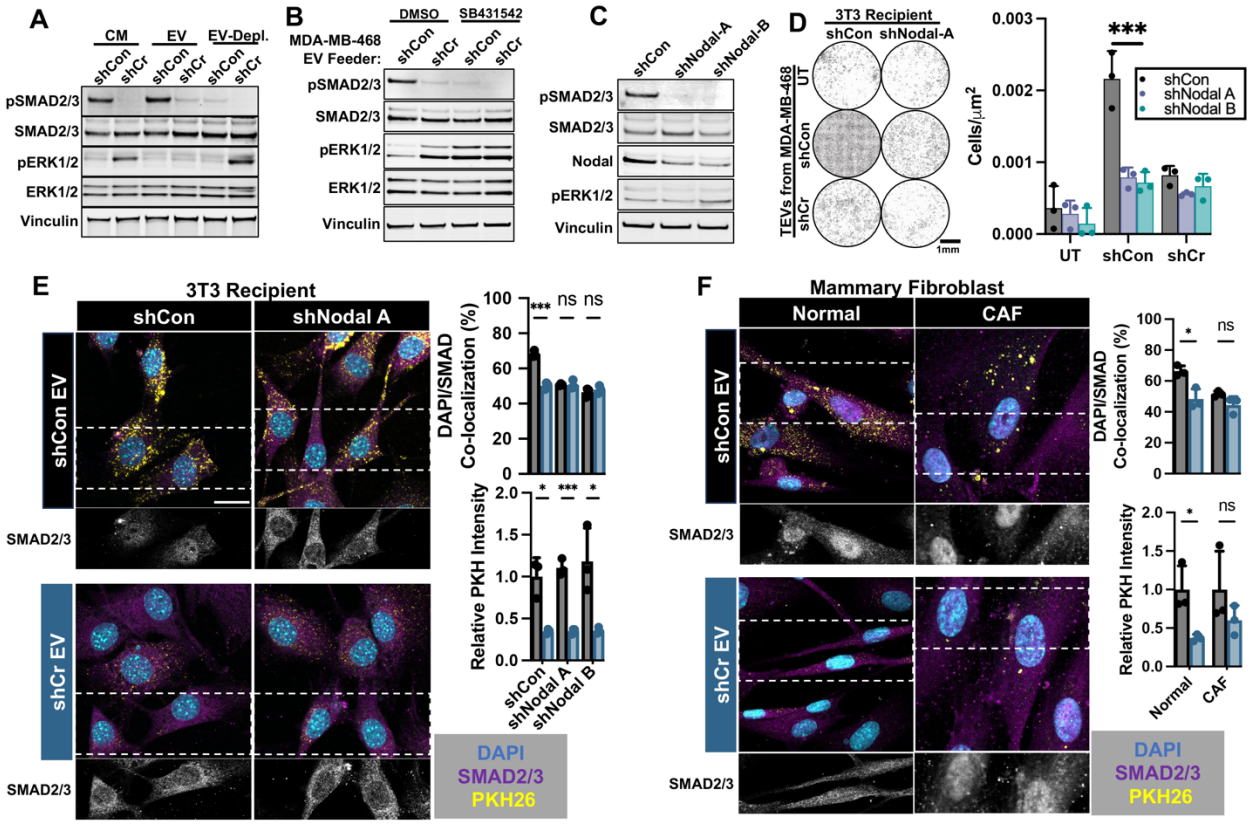

Figure 4. CRIPTO promotes SMAD activation and EV uptake in fibroblasts through discrete NODAL-dependent and –independent pathways
Western blots of 3T3s treated with (A) conditioned media (CM), TEVs or TEV-depleted media (EV-depl) collected from shCon and shCr MDA-MB-468 cells and (B) TEVs from MDA-MB-468 shCon or shCr cells in addition to treatment with SB431542 (10uM, 16hrs). (C) Western blot of shCon and NODAL knockdown (shNODAL) in 3T3s treated with TEVs from MDA-MB-468 shCon cells. (D) Invasion assay of MDA-MB-468 cells cultured above shCon or shNODAL 3T3s treated with EVs from MDA-MB-468 shCon or shCr cells. Immunocytochemistry of (E) shCon and shNodal 3T3s and (F) Primary mammary fibroblasts and CAFs treated with PKH26 labeled EVs isolated from MDA-MB-468 shCon or shCr cells. Quantification of nuclear SMAD2/3 and relative PKH intensity on the right (N=3; 4 fields of view/replicate); Holm-Šidák Multiple T-tests. Scale Bar = 20□m. *P<0.05 , **P<0.01, ***P<0.001

CRIPTO-mediated activation of SMAD2/3 typically involves the TGF-β family ligand NODAL and NODAL has previously been associated with active CAFs in TNBC[27]. We asked whether CRIPTO-expressing TEVs promoted SMAD2/3 activation by facilitating signaling through locally produced NODAL in fibroblasts. We found NODAL knockdown (shNODAL) in recipient fibroblasts blocked SMAD2/3 phosphorylation in fibroblasts treated with TEVs from CRIPTO expressing TNBC cells (**Fig 4C**). These data suggested a model in which tumor cells provide CRIPTO to fibroblasts in the form of CR-laden EVs that then act in concert with fibroblast-expressed NODAL to program fibroblasts to reciprocally promote tumor cell migration. Consistent with this conjecture,

240 fibroblasts treated with isolated shCon TEVs promoted tumor cell invasion and this effect was
241 reversed by knockdown of CRIPTO in the EV-producing tumor cells or by NODAL knockdown in
242 the recipient fibroblasts (**Fig 4D**). These data highlight an intercellular signaling axis dependent
243 on CRIPTO and NODAL expression in separate cell populations.
244
245 We next asked whether TEV uptake was contingent on NODAL expression within fibroblasts.
246 Fluorescently labeled TEVs from shCon cells were taken up equally by control and shNodal
247 fibroblast while TEVs from shCr cells were internalized less readily, regardless of NODAL
248 expression in fibroblasts. In contrast, levels of nuclear SMAD2/3 (indicative of SMAD activation)
249 were dependent on both fibroblast NODAL levels and tumor CRIPTO levels (**Fig 4E**). Critically,
250 the differential EV uptake observed in our 3T3 model system was recapitulated using primary
251 human mammary fibroblasts as the recipient cell type. In primary human fibroblasts, shCon EVs
252 were taken up more readily than shCr EVs and promoted nuclear localization of SMAD2/3 that
253 was diminished when using shCr-donor cell EVs (**Fig 4E**). Thus, CRIPTO regulates EV uptake
254 and SMAD activation through distinct pathways in fibroblasts. Interestingly, patient-derived CAFs
255 showed trends of enhanced TEV uptake from CRIPTO-expressing cells relative to shCR TEV that
256 were similar to 3T3s, though not statistically significant. However, we observed comparable levels
257 of nuclear SMAD localization (indicative of activation) in CAFs treated with shCon TEVs versus
258 those treated with shCr TEVs (**Fig 4F**). Suggesting CAFs, as opposed to normal resident
259 fibroblasts, may have activated secondary mechanisms to sustain SMAD activation
260 independently of CRIPTO-TEV signaling (**Fig 4F**).
261
262 **DISCUSSION**
263 In the TME, non-autonomous signaling drives adaptive responses in both stromal and
264 parenchymal cells, contributing to cancer progression and resistance to treatment[1,16]. Our study
265 uncovers a novel instructive role for tumor cell-derived EVs bearing CRIPTO protein in this

266 dynamic activity. CRIPTO-laden EVs program fibroblasts toward an activated fibroblast cell-state,
267 which in turn enhances tumor cell invasion. This process involves NODAL-dependent activation
268 of SMAD2/3 in recipient fibroblasts and CRIPTO-dependent but NODAL-independent EV uptake.
269 Our prior studies point to stress-dependent activation of CRIPTO signaling in parenchymal
270 cells enhancing tumor cell fitness as a function of GRP78 cell surface localization within stressed
271 tumor microdomains[7]. We show here that such domains also exhibit colocalization of CRIPTO
272 with EV marker CD81 and correlated increases in elongated, αSMA-positive fibroblasts and
273 fibrosis. Chronic exposure of fibroblasts to CRIPTO-bearing EVs drives SMAD activation, the
274 expression of classical CAF markers, and transcriptional changes associated with the TGF-β
275 pathway, matrisome remodeling, and ER stress.
276 Whether CRIPTO's role in autocrine/paracrine signaling via EVs involves the packaging
277 of other pathway components as EV cargo remains to be determined. EVs are known to promote
278 αSMA expression in fibroblasts by transferring latent TGF-β complexes from tumor cells[21].
279 Furthermore, CRIPTO not only facilitates NODAL ALK4 complex formation, but also regulates
280 proper NODAL localization and trafficking via coupling with convertases FURIN and PACE4[28,29].
281 In addition to TGF-β pathways, CRIPTO influences growth factor signaling through c-Src and
282 ERK/AKT pathways[9]. The promotion of ERK activation in target fibroblast cells by non-EV-specific
283 soluble factors that is blocked by CRIPTO-EVs suggests a multifaceted cooperation between cell
284 types and signaling pathways. The restoration of ERK activation by inhibiting ALK4,5,7 indicates
285 EV-based CRIPTO may balance differentiation and proliferation cues to facilitate CAF activation.
286 Our initial indication of CRIPTO's role in modulating fibroblast behavior stems from a
287 correlation between a CAF signature and the prevalence of CRIPTO-regulated tumor populations.
288 This suggests that these tumor populations are key players in the complex interplay of signals
289 between CAFs and tumor cells, highlighting the importance of understanding tumor cell
290 heterogeneity and the nuanced "call and response" mechanisms driving tumor progression. We

291 also noted the correlation of CRIPTO populations with a $CD4^+$ T cell signature. The basis of this
292 relationship will require further investigation, but we note that CAFs have been reported to alter
293 intratumoral immune cell levels through cytokine secretion and alteration of the mechanical profile
294 of the extracellular matrix[30,31]. Whether CRIPTO activity influences immune components of the
295 TME directly or through altered CAF activity presents intriguing avenues for future research,
296 especially regarding CRIPTO inhibition's potential synergy with immune checkpoint blockade.

297 Our study utilizes various cell lines and patient-derived TNBC models highlighting elevated
298 CRIPTO activity in this subtype. However, the findings are potentially relevant to other breast
299 cancer subtypes or cancers in other tissues with significant fibroblast involvement, such as lung,
300 liver, prostate, and pancreatic cancer. Indeed, CRIPTO overexpression has been reported in a
301 broad spectrum of breast cancers, including hormone receptor (HR+) and HER2+ tumors in
302 addition to TNBC[5]. Further, CRIPTO/GRP78 signaling has now been implicated in an array of
303 tumor types outside of the mammary system[32,33].

304 EVs from MDA-MB-231 sublines prime pre-metastatic niches, specifically targeting cells,
305 including S100A4+ lung fibroblasts through differential integrin expression[19]. Here we report for
306 the first time that modulation of CRIPTO expression in tumor cells significantly changes EV uptake
307 rates and cellular programming of recipient cells both *in vitro* and *in vivo*. This discovery of may
308 open new avenues for therapy development by blocking critical CRIPTO-EV's role in modifying
309 stromal fibroblasts. Previous efforts to target the tumor microenvironment (TME) and CAFs in
310 breast cancer, particularly using TGF-β inhibitors, have failed early clinical trials due to significant
311 off-target toxicities[34]. In contrast, CRIPTO, minimally expressed in normal adult tissue, could
312 present a safer target, with previous *in vivo* targeting showing no adverse effects[7,35]. This could
313 be especially valuable in the TNBC subtype that currently has limited targeted therapies, with
314 significant implications for developingt therapies.

315 In conclusion, our study establishes CRIPTO as a pivotal component of heterotypic
316 tumor:fibroblast signaling within TNBC, with potential biologic and therapeutic relevance to other

317 cancers via its role in modulating EV internalization and signaling within the TME. While significant
318 advances have been made in targeting the immune stromal component of the microenvironment,
319 limited inroads have been made in targeting CAFs in breast cancer despite their prevalence and
320 critical roles. By targeting tumor-supportive CAFs, it may be possible to dampen mechanisms of
321 resistance, and therefore, CRIPTO-directed therapies may prove to be important players in
322 combinatorial therapeutic approaches. Collectively, these data have implications for biomarker
323 and therapeutic target discovery.
324

325 **METHODS**

326 *Cell culture*

327 MDA-MB-468, MDA-MB-231 and NIH-3T3 cells were acquired from ATCC. Cells were cultured in
328 'Tumor Media' (Dulbecco's modified Eagle's media (DMEM), 10% fetal bovine serum, and
329 ciprofloxacin 10□g/mL). NIH-3T3 cells were treated with 1□g/mL of mitomycin-C for 2 hours to
330 generate growth arrested fibroblasts. For treatments with inhibitors or EVs, cells were cultured
331 with media containing EV-depleted FBS for 24 hours prior to treatment. PDxOs were a generous
332 gift from the Welm Labs (HCI) and were cultured according to their published protocol[36]. Primary
333 human mammary fibroblasts and CAFs were aquired from Cell Biologics and cultured in tumor
334 media tumor media supplemented with FGF (100ng/mL) and hydrocortisone (1□g/mL).
335

336 *RNA-sequencing*

337 For scRNA-seq MDA-MB-468 expressing either s14-Con or s14-A4 were grown as organoids in
338 low adhesion plates with 5% Engelbreth-Holm-Swarm (EHS)-derived basement membrane matrix
339 for 7 days. Organoids were trypsinized, dissociated with dispase and barcoded with the Chromium
340 Next GEM Single Cell 3' Kit v3.1 with cell multiplexing according to the manufacturer's instructions
341 [Protocol #1] (#100261, 10X Genomics, Pleasanton, CA). Sequencing was performed on the

342 NovaSeq 6000 with 150x150 paired end mode by the University of Utah High Throughput
343 Genomics Core (HTGC) at Huntsman Cancer Institute based on the 10X genomics user guide
344 (CG000315).
345 For bulk RNAsequencing, NIH/3T3s were cultured in EV-depleted tumor media and treated with
346 2.5□g of purified EVs from MDA-MB-468 shCon, shCripto, or CRIPTO overexpressing cells for 24
347 hours. RNA was collected with RNeasy Kit according the manufacturer's instructions (#74104,
348 Qiagen, Germantown, MD) and purity was validated using a 2100 Bioanylyzer (Agilent
349 Technologies, Santa Clara, CA) and Qubit™ Broad Range RNA kit (Thermo Fisher Scientific,
350 Waltham, MA). Libraries were prepped with the NEBNext Ultra II Directional RNA library Prep with
351 Poly(A) isolation (New England Biolabs, Ipswich, MA). Reads were aligned to the mouse genome
352 using Elysium. We quantified gene expression as transcripts per million (TPM).
353
354 *Lentiviral Vectors:*
355 S14-Con and -A4 lentiviral expression vectors are previously described tet-inducible constructs[7].
356 *TDGF1* and *NODAL* knockdown constructs were purchased from Horizon Discovery and Origene
357 respectively.
358
359 *Immunofluorescence*
360 Cells were cultured on 8-well chamber slides with removable covers (#155409PK, Thermo Fisher
361 Scientific, Waltham, MA). Upon culture endpoint cells were fixed with 4% PFA, permeabilized with
362 0.05% Triton-X 100, and blocked with 10% goat serum. For EV internalization, cells were
363 incubated with 1□g of PKH26-labeled EVs for 1 hour prior to fixation. Permeabilized cells were
364 probed for SMAD2/3 (#AF3797, R&D Biosystems, 10□g/mL) and imaged on an SP8 white laser
365 confocal microscope (Leica Biosystems, Wetzlar, Germany).
366

367 *Microwell Organoid Assay*

368 MDA-MB-468 and mitomycin-C treated NIH-3T3 cells were plated at a ratio of 10:1 in
369 AggreWell^{TM}400 plates at approximately 50 cells/microwell according to the manufacturer's
370 instructions (#34415, Stemcell Technologies, Vancouver, BC) and grown for 5 days in tumor
371 media containing 1□g/mL doxycycline. Dispersed cell counts were measured blinded as the
372 number of cells present beyond the average diameter of MDA-MB-468 monoculture spheroids
373 using the image analysis software FIJI[37].

374

375 *Western Blots*

376 Cells and EVs were lysed in RIPA buffer supplemented with protease/phosphatase inhibitors
377 (#78440, Thermo Fisher Scientific, Waltham, MA) and quantified with DC Protein Assay (#500111,
378 BioRad, Hercules, CA). Lysates were boiled in LDS loading buffer with 0.1M DTT and run on 4-
379 12% precast Bis-Tris gels (NP0336BOX, Thermo Fisher Scientific, Waltham, MA). Proteins were
380 transferred using an iBlot2 transfer device (Thermo Fisher Scientific, Waltham, MA), blocked with
381 Intercept Blocking Buffer (927-7001, LiCor Biosciences, Lincoln, NE), and immunoblotted with the
382 following antibodies: phospho-SMAD2 (Ser465/467)/SMAD3 (Ser423/425) (Clone D27F4, Cell
383 Signaling, 1:1000), SMAD2/3 (#AF3797, R&D Biosystems, 0.5□g/mL), Phospho-ERK1/2
384 (Thr202/204) (Clone D13.144E, Cell Signaling, 1:1000), ERK1/2 (L34F12, Cell Signaling,
385 1:2000), Vinculin (Clone EPR8185, Abcam, 1:1000), Calnexin (Clone C5C9, Cell Signaling,
386 1:1000), HSP70 (#4872, Cell Signaling, 1:1000), Flotillin-1 (Clone D2V7J, Cell Signaling, 1:1000),
387 CD81 (Clone D3N2D, Cell Signaling, 1:1000), NODAL (Clone WS65, Santa Cruz Biotechnology,
388 1:200), Goat anti-rabbit IgG AF680 (#A21076, Thermo Fisher Scientific, 1:2000), Donkey anti-
389 goat IgG AF800 (#A32930, Thermo Fisher Scientific, 1:2000), Goat anti-mouse IgG (#A11375,
390 Thermo Fisher Scientific, 1:2000).

391

392 *PCR*

393 RNA was isolated from cells using the RNeasy Kit (#74104, Qiagen, Germantown, MD) and
394 quantified on a NanoDrop 8000 (Thermo Fisher Scientific, Waltham, MA). RT-qPCR was
395 performed using PowerUp™ Sybr™ Green Master Mix (#A25741, Thermo Fisher Scientific,
396 Waltham, MA) according to manufacturer's protocol and utilized a BioRad™ CFX384
397 thermocycler. Comparisons were made using the following pre-validated housekeeping genes:
398 *POLR2A* (Hs.PT.39a.19639531; IDT, San Diego, CA); *Polr2a* (MM.PT.39a.22214849; IDT, San
399 Diego, CA). The following custom RNA-specific primer sequences were designed: *TDGF1:*
400 (Forward: TCCTTTTGTGCCTGCCCTC Reverse: CACAGGGAACACTTCTTGG); *SOSTDC1*
401 (Forward: TCAAGCCAGAAATGGAGGCAGG Reverse: GCCATCAGAGATGTATTTGGTGG);
402 *CRYAB* (Forward: ACTTCCCTGAGTCCCTTCTACC Reverse:
403 GGAGAAGTGCTTCACATCCAGG); *Tnc* (Forward: GAGACCTGACACGGAGTATGAG Reverse:
404 CTCCAAGGTGATGCTGTTGTCTG); *TGF-β* (Forward: TGATACGCCTGAGTGGCTGTCT
405 Reverse: CACAAGAGCAGTGAGCGCTGAA); *S100a4* (Forward:
406 AGCTCAAGGAGCTACTGACCAG Reverse: GCTGTCCAAGTTGCTCATCACC); *Pdgfrα*
407 (Forward: GCAGTTGCCTTACGACTCCAGA Reverse: GGTTTGAGCATCTTCACAGCCAC); *Fn1*
408 (Forward: CCCTATCTCTGATACCGTTGTCC Reverse: TGCCGCAACTACTGTGATTCGG); *Fap*
409 (Forward: CCCGCGTAACACAGGATTCACT Reverse: CACACTTCTTGCTCGGAGGAGA);
410 *Acta2* (Forward: CACTATTGGCAACGAGCGC Reverse: CCAATGAAGGAAGGCTGGAA).

411

412 *Invasion Assays*

413 Invasion assays were performed using 6.5mm polycarbonate membrane Transwell® inserts with
414 8.0□m pores. Inserts were coated with 45□L of EHS basement membrane matrix and solidified at
415 37C for 5 minutes[38]. 2.0×10^4 tumor cells plated in 100□□L on top of the EHS coated insert were
416 grown with fibroblasts for 72 hours to prime fibroblasts. Priming inserts were discarded and fresh

417 EHS coated inserts with $2.0x10^4$ tumor cells were placed on top of both naïve and primed
418 fibroblasts and cultured for an additional 48 and 72 hours for cell lines and PDxOs, respectively.
419 Inserts were washed with PBS, fixed with 4% PFA for 15 minutes at RT, permeabilized with 0.05%
420 Triton X-100, incubated with DAPI 1 g/mL for 5 minutes. EHS matrix/non-migrated cells were
421 removed from the top of the transwell with a cotton tipped applicator following permeabilization.
422 Membranes were excised, mounted, and coverslipped in ProLong™ Gold mounting media
423 (#P36930, Thermo Fisher Scientific, Waltham, MA), and imaged on an Axioscan 7 Slide Scanner
424 (Zeiss, Oberkochen, Germany). Membrane area was manually measured and DAPI counts were
425 performed using the automated cell counting program in QuPath[39].
426
427 *Extracellular Vesicle Isolation and labeling*
428 EVs were isolated by differential ultracentrifugation as previously described and validated
429 according to recent MISEV2023 guidlines[25,40]. Cells were cultured at 70-90% confluency for 48
430 hours in Tumor Media with EV-depleted FBS. Conditioned media was collected and subjected to
431 sequential centrifugation at 500g for 10 minutes, 2500g for 20 minutes, 10000g for 30 minutes,
432 passed through 0.2 m PES filters and centrifuged at 120,000g for 2 hours (SW28 rotor, K=246).
433 Pelleted EVs were resuspended in 0.2 m filtered PBS and centrifuged at 120,000g for 2 hours
434 (SW55Ti rotor, K=48). The resulting EV pellet was resuspended in either filtered PBS or RIPA
435 depending on downstream assays. For PKH26 staining, isolated EVs were labeled according to
436 the manufacturer's instructions (MIDI6-1KT, Sigma, Burlington, MA). Excess PKH was removed
437 by centrifugation at 190,000g for 2 hours with a 0.971M sucrose cushion (SW55Ti rotor, K=48).
438 EVs were resuspended in 9mL of PBS and filtered with a 10kDa centrifugal filter (UFC901008,
439 Sigma, Burlington, MA) at 3000g for 30 minutes. PKH26 labeled EVs were stored at 4C and used
440 within 24 hours of labeling.
441

442 *Nanoparticle Tracking Analysis*

443 EV samples were diluted 1:20 with 0.2□m filtered PBS. Size distribution and concentration were
444 analyzed on a NS300 (Malvern, Malvern UK). Samples were recorded blinded over 3 videos of
445 60s at detection threshold: 3, camera level: 13 with a coefficient of variance of <15%.

446

447 *Electron Microscopy*

448 EVs were applied (3.5 µL) to glow-discharged 2/1 Quantifoil carbon 300-mesh Cu grids. Grids
449 were blotted for 4-6 seconds on the front-side of the grid and immediately plunged into liquid
450 Ethane using a Leica plunge freezing device.

451

452 *EV Uptake Timecourse*

453 Cells were grown in 8 well chambered coverglass (#155409, Thermo Fisher Scientific, Waltham,
454 MA) and imaged with an SP8 white laser confocal (Leica Biosystems, Wetzlar, Germany) with a
455 stage top incubator (Okolab, Sewickley, PA). Two images per well were taken at 200X
456 magnification in 20 minutes intervals over an 8 hour period. 1□g of PKH26-labeled EVs were
457 added after an initial image and fluorescence intensity was normalized based on the fluorescent
458 EV signal after the secod timepoint for each condition.

459

460 *In Vivo Studies*

461 10-12 week old SCID-Beige mice were purchased from Charles River Laboratory (Wilmington,
462 MA). All animal care and procedures were approved and monitored by an Institutional Animal
463 Care and Use Committee. For EV uptake studies, mice received retroorbital injections of 10□g of
464 PKH26 (MIDI6-1KT, Sigma, Burlington, MA) labeled EV as previously described[19]. 24 hours
465 following EV administration, animals were euthanized, and lungs and livers were harvested, fixed
466 in 4% PFA overnight followed by sequential incubation in 10% sucrose (1 hour), 20% sucrose (1

467 hour), and 30% sucrose (overnight) solutions. Fixed tissues were embedded in O.C.T, frozen, and
468 cryosectioned at 5□m.
469
470 ACKNOWLEDGMENTS
471 We would like to thank the cell imaging, electron microscopy, and high throughput genomics cores
472 at HCI for their expertise and equipment, and R. O'Connell for generous use of the nanosight.
473
474 AUTHOR CONTRIBUTIONS
475 Concept and writing: DWF and BTS wrote the manuscript with input from all the authors. DWF
476 and BTS conceived and designed the study, and DWF and BLG conducted the experiments. HEG
477 and MDS performed blinded analysis of PDX sections and microwell assays, respectively.
478
479 FUNDING
480 Portions of this work were supported by the Department of Defense BCRP (BC201559), the
481 Huntsman Cancer Foundation, an NIH-NICHD training grant (T32HD007491) and an NIH CCSG
482 support grant (P30 CA42014). The content is solely the responsibility of the authors and does not
483 necessarily represent the official views of the NIH.

REFERENCES

1 Sahai, E. *et al.* A framework for advancing our understanding of cancer-associated fibroblasts. *Nat Rev Cancer* **20**, 174-186 (2020). https://doi.org:10.1038/s41568-019-0238-1

2 Freeman, D. W. *et al.* Whence CRIPTO: The Reemergence of an Oncofetal Factor in 'Wounds' That Fail to Heal. *Int J Mol Sci* **22** (2021). https://doi.org:10.3390/ijms221810164

3 Spike, B. T. *et al.* CRIPTO/GRP78 signaling maintains fetal and adult mammary stem cells ex vivo. *Stem Cell Reports* **2**, 427-439 (2014). https://doi.org:10.1016/j.stemcr.2014.02.010

4 Dublin, E., Bobrow, L., Barnes, D. & Gullick, W. Amphiregulin and cripto overexpression in breast-cancer - relationship with prognosis and clinical and molecular-variables. *Int J Oncol* **7**, 617-622 (1995). https://doi.org:10.3892/ijo.7.3.617

5 Gong, Y. P. *et al.* Overexpression of Cripto and its prognostic significance in breast cancer: a study with long-term survival. *Eur J Surg Oncol* **33**, 438-443 (2007). https://doi.org:10.1016/j.ejso.2006.10.014

6 Bianco, C. *et al.* Role of Cripto-1 in stem cell maintenance and malignant progression. *Am J Pathol* **177**, 532-540 (2010). https://doi.org:10.2353/ajpath.2010.100102

7 Balcioglu, O. *et al.* CRIPTO antagonist ALK4(L75A)-Fc inhibits breast cancer cell plasticity and adaptation to stress. *Breast Cancer Res* **22**, 125 (2020). https://doi.org:10.1186/s13058-020-01361-z

8 Klauzinska, M. *et al.* The multifaceted role of the embryonic gene Cripto-1 in cancer, stem cells and epithelial-mesenchymal transition. *Semin Cancer Biol* **29**, 51-58 (2014). https://doi.org:10.1016/j.semcancer.2014.08.003

9 Bianco, C. *et al.* A Nodal- and ALK4-independent signaling pathway activated by Cripto-1 through Glypican-1 and c-Src. *Cancer Res* **63**, 1192-1197 (2003).

10 Bianco, C. *et al.* Cripto-1 activates nodal- and ALK4-dependent and -independent signaling pathways in mammary epithelial Cells. *Mol Cell Biol* **22**, 2586-2597 (2002). https://doi.org:10.1128/MCB.22.8.2586-2597.2002

11 Gray, P. C., Harrison, C. A. & Vale, W. Cripto forms a complex with activin and type II activin receptors and can block activin signaling. *Proc Natl Acad Sci U S A* **100**, 5193-5198 (2003). https://doi.org:10.1073/pnas.0531290100

12 Gray, P. C., Shani, G., Aung, K., Kelber, J. & Vale, W. Cripto binds transforming growth factor beta (TGF-beta) and inhibits TGF-beta signaling. *Mol Cell Biol* **26**, 9268-9278 (2006). https://doi.org:10.1128/MCB.01168-06

13 Shani, G. *et al.* GRP78 and Cripto form a complex at the cell surface and collaborate to inhibit transforming growth factor beta signaling and enhance cell growth. *Mol Cell Biol* **28**, 666-677 (2008). https://doi.org:10.1128/MCB.01716-07

14 Karkampouna, S. *et al.* Oncofetal Protein CRIPTO Is Involved in Wound Healing and Fibrogenesis in the Regenerating Liver and Is Associated with the Initial Stages of Cardiac Fibrosis. *Cells* **10** (2021). https://doi.org:10.3390/cells10123325

15 Tchou, J. *et al.* Human breast cancer associated fibroblasts exhibit subtype specific gene expression profiles. *BMC Med Genomics* **5**, 39 (2012). https://doi.org:10.1186/1755-8794-5-39

16 Bartoschek, M. *et al.* Spatially and functionally distinct subclasses of breast cancer-associated fibroblasts revealed by single cell RNA sequencing. *Nat Commun* **9**, 5150 (2018). https://doi.org:10.1038/s41467-018-07582-3

17 Sun, K. *et al.* Oxidized ATM-mediated glycolysis enhancement in breast cancer-associated fibroblasts contributes to tumor invasion through lactate as metabolic coupling. *EBioMedicine* **41**, 370-383 (2019). https://doi.org:10.1016/j.ebiom.2019.02.025

18 van Niel, G., D'Angelo, G. & Raposo, G. Shedding light on the cell biology of extracellular vesicles. *Nat Rev Mol Cell Biol* **19**, 213-228 (2018). https://doi.org:10.1038/nrm.2017.125

19 Hoshino, A. *et al.* Tumour exosome integrins determine organotropic metastasis. *Nature* **527**, 329-335 (2015). https://doi.org:10.1038/nature15756

20 Hu, C. *et al.* Exosomal Cripto-1 Serves as a Potential Biomarker for Perihilar Cholangiocarcinoma. *Front Oncol* **11**, 730615 (2021). https://doi.org:10.3389/fonc.2021.730615

21 Webber, J., Steadman, R., Mason, M. D., Tabi, Z. & Clayton, A. Cancer exosomes trigger fibroblast to myofibroblast differentiation. *Cancer Res* **70**, 9621-9630 (2010). https://doi.org:10.1158/0008-5472.CAN-10-1722

22 Mercier, I. *et al.* Human breast cancer-associated fibroblasts (CAFs) show caveolin-1 downregulation and RB tumor suppressor functional inactivation: Implications for the response to hormonal therapy. *Cancer Biol Ther* **7**, 1212-1225 (2008). https://doi.org:10.4161/cbt.7.8.6220

23 Yao, J., Li, S. & Wang, X. Identification of Breast Cancer Immune Subtypes by Analyzing Bulk Tumor and Single Cell Transcriptomes. *Front Cell Dev Biol* **9**, 781848 (2021). https://doi.org:10.3389/fcell.2021.781848

24 Mantile, F. *et al.* A Novel Localization in Human Large Extracellular Vesicles for the EGF-CFC Founder Member CRIPTO and Its Biological and Therapeutic Implications. *Cancers (Basel)* **14** (2022). https://doi.org:10.3390/cancers14153700

25 Welsh, J. A. *et al.* Minimal information for studies of extracellular vesicles (MISEV2023): From basic to advanced approaches. *J Extracell Vesicles* **13**, e12404 (2024). https://doi.org:10.1002/jev2.12404

26 Kojima, Y. *et al.* Autocrine TGF-beta and stromal cell-derived factor-1 (SDF-1) signaling drives the evolution of tumor-promoting mammary stromal myofibroblasts. *Proc Natl Acad Sci U S A* **107**, 20009-20014 (2010). https://doi.org:10.1073/pnas.1013805107

27 Dieters-Castator, D. *et al.* Embryonic protein NODAL regulates the breast tumor microenvironment by reprogramming cancer-derived secretomes. *Neoplasia* **23**, 375-390 (2021). https://doi.org:10.1016/j.neo.2021.02.004

28 Blanchet, M. H. *et al.* Cripto recruits Furin and PACE4 and controls Nodal trafficking during proteolytic maturation. *EMBO J* **27**, 2580-2591 (2008). https://doi.org:10.1038/emboj.2008.174

29 Blanchet, M. H. *et al.* Cripto localizes Nodal at the limiting membrane of early endosomes. *Sci Signal* **1**, ra13 (2008). https://doi.org:10.1126/scisignal.1165027

30 Kinoshita, N., Minshull, J. & Kirschner, M. W. The identification of two novel ligands of the FGF receptor by a yeast screening method and their activity in Xenopus development. *Cell* **83**, 621-630 (1995). https://doi.org:10.1016/0092-8674(95)90102-7

31 Salmon, H. *et al.* Matrix architecture defines the preferential localization and migration of T cells into the stroma of human lung tumors. *J Clin Invest* **122**, 899-910 (2012). https://doi.org:10.1172/JCI45817

32 Karkampouna, S. *et al.* CRIPTO promotes an aggressive tumour phenotype and resistance to treatment in hepatocellular carcinoma. *The Journal of Pathology* **245**, 297-310 (2018). https://doi.org:10.1002/path.5083

33 Zoni, E. *et al.* CRIPTO and its signaling partner GRP78 drive the metastatic phenotype in human osteotropic prostate cancer. *Oncogene* **36**, 4739-4749 (2017). https://doi.org:10.1038/onc.2017.87

34 Anderton, M. J. *et al.* Induction of heart valve lesions by small-molecule ALK5 inhibitors. *Toxicol Pathol* **39**, 916-924 (2011). https://doi.org:10.1177/0192623311416259

35 Kelly, R. K. *et al.* An antibody-cytotoxic conjugate, BIIB015, is a new targeted therapy for Cripto positive tumours. *Eur J Cancer* **47**, 1736-1746 (2011). https://doi.org:10.1016/j.ejca.2011.02.023

36 Scherer, S. D. *et al.* Breast cancer PDxO cultures for drug discovery and functional precision oncology. *STAR Protoc* **4**, 102402 (2023). https://doi.org:10.1016/j.xpro.2023.102402

37 Schindelin, J. *et al.* Fiji: an open-source platform for biological-image analysis. *Nat Methods* **9**, 676-682 (2012). https://doi.org:10.1038/nmeth.2019

38 DeRose, Y. S. *et al.* Patient-derived models of human breast cancer: protocols for in vitro and in vivo applications in tumor biology and translational medicine. *Curr Protoc Pharmacol* **Chapter 14**, Unit14 23 (2013). https://doi.org:10.1002/0471141755.ph1423s60

39 Bankhead, P. *et al.* QuPath: Open source software for digital pathology image analysis. *Sci Rep* **7**, 16878 (2017). https://doi.org:10.1038/s41598-017-17204-5

40 Kowal, J. *et al.* Proteomic comparison defines novel markers to characterize heterogeneous populations of extracellular vesicle subtypes. *Proc Natl Acad Sci U S A* **113**, E968-977 (2016). https://doi.org:10.1073/pnas.1521230113